

See discussions, stats, and author profiles for this publication at: <https://www.researchgate.net/publication/223971142>

# pH-Responsive Layer-by-Layer Nanoshells for Direct Regulation of Cell Activity

ARTICLE *in* ACS NANO · APRIL 2012

Impact Factor: 12.88 · DOI: 10.1021/nn3008355 · Source: PubMed

---

CITATIONS

41

READS

24

## 7 AUTHORS, INCLUDING:



Irina Drachuk

Air Force Research Laboratory, Wright-Patte...

14 PUBLICATIONS 422 CITATIONS

[SEE PROFILE](#)



Milana Lisunova

Nano3D systems, Santa Clara, CA

33 PUBLICATIONS 518 CITATIONS

[SEE PROFILE](#)



Nancy Kelley-Loughnane

Air Force Research Laboratory

40 PUBLICATIONS 343 CITATIONS

[SEE PROFILE](#)



Morley O Stone

United States Air Force

97 PUBLICATIONS 4,186 CITATIONS

[SEE PROFILE](#)

# pH-Responsive Layer-by-Layer Nanoshells for Direct Regulation of Cell Activity

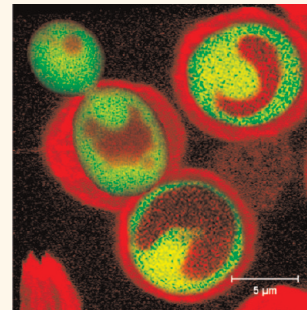
Irina Drachuk,<sup>†</sup> Olga Shchepelina,<sup>†</sup> Milana Lisunova,<sup>†</sup> Svetlana Harbaugh,<sup>‡</sup> Nancy Kelley-Loughnane,<sup>‡</sup> Morley Stone,<sup>‡</sup> and Vladimir V. Tsukruk<sup>†,\*</sup>

<sup>†</sup>School of Materials Science and Engineering, Georgia Institute of Technology, Atlanta, Georgia 30332, United States and <sup>‡</sup>Air Force Research Laboratory, Directorate of Human Effectiveness, Wright-Patterson AFB, Dayton, Ohio 45433, United States

The formation of “smart” biomimetic and environmentally responsive synthetic materials is gaining significant interest for applications in biomedical, bio-sensing, and biotechnological arenas.<sup>1–3</sup> The benefit of having this type of biomaterial lies in the effective control over molecular and cellular interactions at material interfaces.<sup>4</sup> For example, proteins adsorbed on synthetic material surfaces are of particular interest as they are involved in cell attachment, various cellular signaling pathways, and cell function. One of the approaches by which biointerfacial interactions between material surfaces and biomolecules can be changed is through the use of particular stimuli that may alter the secondary structure of the synthetic molecules to modify their binding affinity. This approach is based on the fact that synthetic macromolecules and hybrid composite materials can be manipulated in response to variations in temperature, pH, ionic strength, specific ions or metals, UV irradiation, and electric or magnetic fields.<sup>5–7</sup>

For instance, the most studied synthetic responsive polymers based upon poly(*N*-isopropylacrylamide) (PNIPAM) derivatives undergo a sharp coil–globule transition in water at 32 °C, changing from a hydrophilic state below this temperature to a hydrophobic state above.<sup>8–11</sup> Correspondingly, cell culture growth on such responsive PNIPAM surfaces can be directly associated with “hydrophilic” and “hydrophobic” surface properties, with cells able to attach to PNIPAM at physiological conditions because of its hydrophobicity and being released because of increased hydrophilicity as a result of decreasing temperature.<sup>12,13</sup> The pH-responsive polymers represent another group of stimuli-responsive materials where ionizable functional groups are capable of donating or

**ABSTRACT** *Saccharomyces cerevisiae* yeast cells encapsulated with pH-responsive synthetic nanoshells from lightly cross-linked polymethacrylic acid showed a high viability rate of around 90%, an indication of high biocompatibility of synthetic pH-responsive shells. We demonstrated that increasing pH above the isoelectric point of the polymer shell leads to a delay in growth rate; however, it does not affect the expression of enhanced green fluorescent protein. We suggest that progressive ionization and charge accumulation within the synthetic shells evoke a structural change in the outer shells which affect the membrane transport. This change facilitates the ability to manipulate growth kinetics and functionality of the cells with the surrounding environment. We observed that hollow layer-by-layer nanoshells showed a remarkable degree of reversible swelling/deswelling over a narrow pH range (pH 5.0–6.0), but their assembly directly on the cell surface resulted in the suppression of large dimensional changes. We suggest that the variation in surface charges caused by deprotonation/protonation of carboxylic groups in the nanoshells controlled cell growth and cell function, which can be utilized for external chemical control of cell-based biosensors.



**KEYWORDS:** layer-by-layer assembly · pH-responsive nanoshells · polymethacrylic acid · hydrogel · cell-based biosensors

accepting protons upon environmental pH changes. In this case, electrostatic repulsions between generated charges cause consequent interactions among charged groups, ions and biomolecules. Polyacids, such as poly(acrylic acid) (PAA) and poly(methacrylic acid) (PMAA), with  $pK_a$  values in the range of 5 are of a particular interest since they exhibit rapid transitional changes at physiologically relevant conditions and are considered to be biocompatible.<sup>14,15</sup> Intracellular biomolecular delivery of drugs using masked pH-responsive compounds has been demonstrated,<sup>16</sup> while pH switching for the control over protein adsorption or cell attachment has started to gain great attention recently.<sup>17</sup>

\* Address correspondence to vladimir@mse.gatech.edu.

Received for review February 24, 2012 and accepted April 10, 2012.

Published online April 10, 2012  
10.1021/nn3008355

© 2012 American Chemical Society

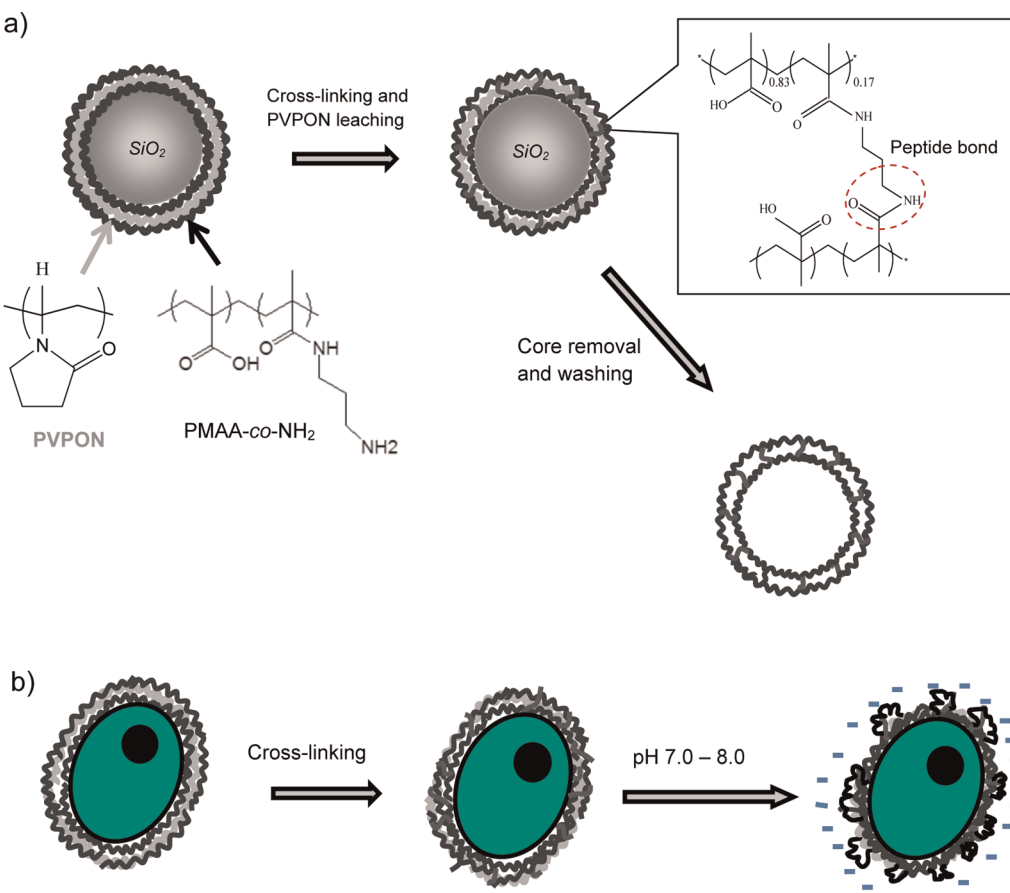


**Figure 1.** LbL self-assembly cross-linked hollow PMAA-co-NH<sub>2</sub> microcapsules *via* amide bonding on sacrificial silica cores (a) and nanoshells on yeast cells (b).

Numerous stimuli-responsive surfaces and interfaces were developed by introducing ionizable groups into the backbone of macromolecules.<sup>18,19</sup> Another approach to produce stimuli-responsive materials involves the formation of gels by physical and/or chemical cross-linking or by supramolecular association of molecular chains dispersed in solvents.<sup>20,21</sup> Hydrogels are of particular interest since their porous net-like structure is filled with a large amount of water, which resembles biological structures. The layer-by-layer (LbL) approach represents an alternative way of creating stimuli-responsive multilayer systems in which chemical species with opposite charges, hydrogen-bonding interactions, or a combination thereof are assembled in an alternating fashion.<sup>22–24</sup> The advantage of this method is the versatility of the template chemistry, its structure and geometry, variation in the thickness of multilayered structures, and the possibility of creating complex multi-responsive sandwich structures.<sup>25,26</sup> The pH-sensitive LbL hydrogels with incorporated quantum dots, gold nanoparticles, and gold nanorods have been demonstrated to be able to act as responsive materials with a strong optical reporting function.<sup>27–29</sup>

In particular, many attempts have been undertaken to use ultrathin LbL nanoshells for the controlled

encapsulation of cells in order to create protected cells and cell assemblies, fabricate cell replicas, biosensing arrays, and to mediate transport properties of biomolecules.<sup>30–37</sup> Although it has been demonstrated that different LbL shells can be readily assembled onto a variety of cells, the issue of cell viability in the presence of cationic components was indicated and suggested to be minimized by the use of hydrogen-bonded shells with minimal or no cationic polymers or by the utilization of natural materials such as silk derivatives.<sup>38–43</sup> In these cases, very high viability reaching 94% in *in vitro* and *in vivo* conditions has been reported. However, LbL shells reported to date have not proven to be robust under variable environmental conditions and not capable of significant and controlled variations of their state. Thus, synthetic nanoshells currently play a passive role in cell growth, interactions, and function. However, no examples of responsive synthetic nanoshells which can serve as an active barrier/coating to control cell function in biosensing devices have been reported to date.

In this paper, we describe a facile strategy for the design of robust but pH-responsive and compliant one-component LbL nanoshells based upon cross-linkable hydrogel PMAA copolymer for controlling the cell function and the rate of proliferation (Figure 1).

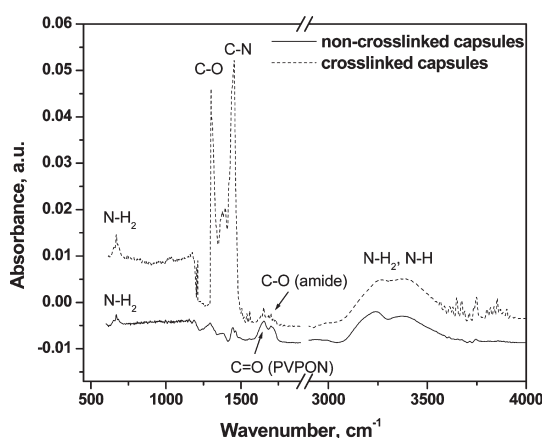


**Figure 2.** ATR-FTIR spectra of un-cross-linked (solid line) and cross-linked for 40 min (dashed line) ( $\text{PMAA-co-NH}_2)_5$  microcapsules (pH 3.5).

The high viability rate of encapsulated cells, which reaches 90%, was related to the elastic nature of the cross-linked and highly porous hydrogel shells with thicknesses of a few tens of nanometers and very minor content of a cationic component. In this strategy, the incorporation of a small amount of amine functional groups into the backbone of the responsive PMAA component allowed the creation of strong amide bonding using the zero-length coupling agent, 1-ethyl-3-(3-dimethylaminopropyl)carbodiimide (EDC), without adverse effects on cell viability.<sup>15</sup> An important finding is that the responsive nature of LbL shells allowed for the control of cell growth and function by changing the external pH environment.

## RESULTS AND DISCUSSION

**Chemical Composition of Model Capsules.** To confirm the chemical composition of cross-linked single-component PMAA- $\text{co-NH}_2$  capsules fabricated in this study (Figure 1), we conducted attenuated total reflection Fourier transform infrared (ATR-FTIR) measurements before and after the cross-linking reaction. Figure 2 demonstrates ATR-FTIR spectra of the un-cross-linked and cross-linked capsules. In both spectra, there are two broad absorption peaks between 3000 and 3500  $\text{cm}^{-1}$  that are characteristic of N–H stretching in primary amines.<sup>44</sup> The NH<sub>2</sub> wagging vibrations are also present at 680  $\text{cm}^{-1}$  for both types of capsules. The very distinct sharp peak centered around 1456  $\text{cm}^{-1}$  in the cross-linked spectrum can be assigned to C–N stretching and N–H bending and provides the necessary evidence for peptide bonding.<sup>45</sup> The presence of this peak is a distinctive feature of amide bonding associated with EDC cross-linking within the PMAA- $\text{co-NH}_2$  shell. It is worth mentioning that the second distinctive peak centered at  $\sim$ 1303  $\text{cm}^{-1}$  was also observed and can be attributed to a complex mixing of C–N stretching, N–H bending, and C–H deformation of amide III from peptide bonding.<sup>48</sup> From the

intensity of both peaks, it can be inferred that carboxylic groups were activated during the coupling process.

In the FTIR spectrum for un-cross-linked capsules, there were two broad closely placed peaks in the range of 1625–1770  $\text{cm}^{-1}$ . The 1720  $\text{cm}^{-1}$  peak is related to protonated carboxylic groups,<sup>46</sup> and the 1660  $\text{cm}^{-1}$  peak is associated with C=O stretching vibrations in PVPON.<sup>47,58</sup> After cross-linking, both peaks were diminished, indicating that a significant amount of PVPON was released (peak 1660  $\text{cm}^{-1}$ ) and the contribution of carboxylic groups was reduced. In addition to this peak, closely placed minor absorption peaks at 1560–1565  $\text{cm}^{-1}$  can be associated with additional N–H bending from the amide II band.<sup>48,49</sup> These data confirmed the formation of partially cross-linked one-component ( $\text{PMAA-co-NH}_2)_5$  shells upon activation with a coupling agent. The large fraction of residual nonreacted carboxylic groups remained free and thus provided sites for the reversible conversion from the protonated to ionized form when exposed to higher pH values responsible for the significant swelling of capsules as discussed below.

**Swelling Behavior and Estimation of the Polymer Mesh Size.** The formation of hydrogen-bonded LbL capsules based on PMAA and amine-functionalized neutral polymer was first reported by the Sukhishvili group, where they produced a highly cross-linked hydrogel network.<sup>58</sup> The time of cross-linking reported in these studies was many hours, reaching 13 h in some cases.<sup>50,51,58</sup> In contrast, in our work, the time for cross-linking within copolymerized PMAA multilayers was specifically set for much lower values to achieve stable capsules with minimum exposure to a highly reactive coupling agent which generates toxic byproducts during the reaction.<sup>52</sup> In our study, we obtained highly stable, single-component PMAA- $\text{co-NH}_2$  capsules with reversible swelling using very mild concentrations of the coupling agent (5 mg/mL) and by reducing the time of cross-linking to only 40 min.

As known, the ability of a polymer network to swell is defined by the molecular weight between cross-links,  $M_c$ , which can be as low as 960 Da for highly cross-linked shells.<sup>53</sup> The change in the network swelling of polymer capsules as a function of pH is related to a change in the mesh size of the gel.<sup>54,58</sup> For our shells, the mesh size was determined from the equilibrium swelling data by calculating  $M_c$  (see Supporting Information).<sup>53</sup> Using  $pK_a = 5.0$  and ionic strength  $I = 0.01$ , the calculations yielded  $M_c = 9500$  Da or about 100 monomeric units between the cross-links, a very low cross-linking density which should facilitate a high swelling ratio. Thus, with 17% of amine content, on average, every sixth unit of the PMAA- $\text{co-NH}_2$  chains is amine-functionalized, out of which only every sixteenth unit of the polymer backbone is actually cross-linked.

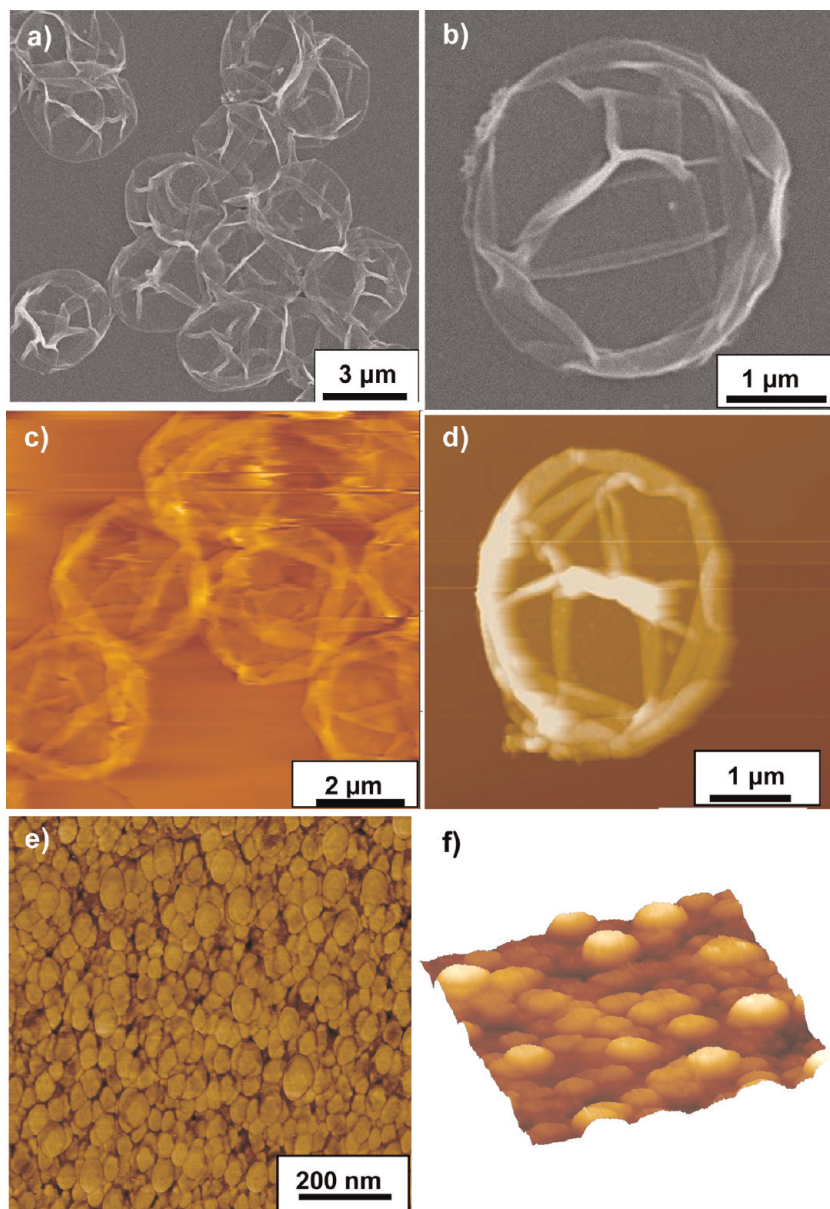


**Figure 3.** SEM images of cross-linked for 40 min  $(\text{PMAA}-\text{co}-\text{NH}_2)_5$  capsules in the dry state (a,b) and AFM images of the capsules in the swollen state at pH 2.0 (c) (Z-scale is 1  $\mu\text{m}$ ) and in the dry state (d) (Z-scale is 350 nm); (e,f) 500 nm  $\times$  500 nm, Z-scale is 20 nm. Image (c) has been taken in contact mode using a liquid cell. Images d–f have been taken in light tapping mode. The close-up view in 3D of the surface morphology in the dry state is represented in panel f. Images c and d are the height, and images e and f are the phase of  $(\text{PMAA}-\text{co}-\text{NH}_2)_5$  capsules.

**Morphology of Microcapsules in the Swollen State.** Figure 3 displays surface morphology of different microcapsules in dry and wet states. Upon drying on a freshly prepared silicon surface, capsules undergo collapse due to evaporation of the aqueous solution, resulting in randomly folded morphologies.<sup>55</sup> Even after post-exposure to aqueous solutions, the swollen capsules preserved the folded structure; however, the increased shell thickness indicates a hydrogel-type swelling response to the presence of a good solvent. By measuring the height of flat regions, which represent folded double-shell regions, the shell thickness of the capsules can be estimated (Figure 4).<sup>55</sup> The dried capsules

were reswollen in aqueous solutions at specified pH values for sufficient time (more than 20 min) to allow them to stabilize before conducting in-liquid AFM scanning.

The capsules possess a characteristic grainy texture (Figures 3 and 4). The values of surface microroughness (calculated here and below for 300 nm  $\times$  300 nm surface areas selected far from wrinkles) are in the range of 2.6–5.1 nm, which are significantly higher than common values for ionic-based LbL shells (usually well below 1 nm).<sup>56,57</sup> In addition, as the time of cross-linking increased from 20 to 40 min, the capsule micro-roughness decreased from  $4.7 \pm 1.1$  to  $2.6 \pm 0.7$  nm,

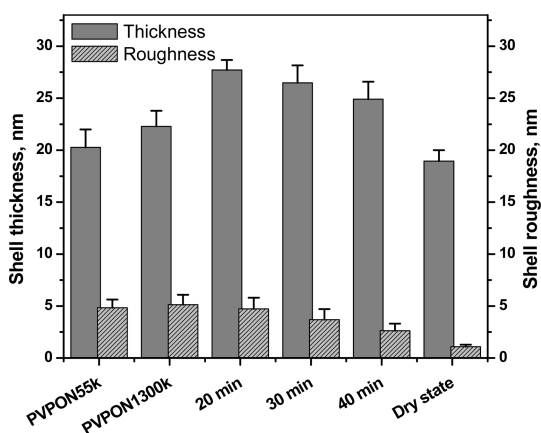


**Figure 4.** Comparison of the thickness and microroughness of un-cross-linked ( $(\text{PVPON}/\text{PMAA})_5$ ) microcapsules with different molecular weight of PVPON ( $M_w = 55 \text{ kDa}$  and  $M_w = 1300 \text{ kDa}$ ) in the swollen state and cross-linked ( $(\text{PMAA}-\text{co}-\text{NH}_2)_5$ ) capsules for different times in the swollen states as well as cross-linked for 40 min in the dry state. All capsules were drop-casted and air-dried from pH 3.5. Data shown are the average with standard deviation ( $n = 15$ ).

indicating reduced porosity. The higher microroughness is a distinctive feature of hydrogen-bonded LbL films, which is associated with the intramolecular aggregation of the components during LbL assembly and the presence of a highly porous morphology.<sup>55</sup>

The analysis of shell thickness and microroughness of cross-linked ( $(\text{PMAA}-\text{co}-\text{NH}_2)_5$ ) capsules in dry and swollen states revealed that in the swollen state microcapsules were 25% thicker ( $25.5 \pm 0.9 \text{ nm}$ ) at low pH as compared to the same capsules in dry state ( $18.9 \pm 1.1 \text{ nm}$ ) (Figure 4). Significantly higher swelling ratio ( $\sim 100\%$ ) was demonstrated by the Sukhishvili group for the high cross-linking density PMAA capsules (the reaction time set for 13 h).<sup>58</sup> In our case, cross-linked capsules in the swollen state at pH 2.0 were  $\sim 10\%$  thicker ( $27.7 \pm 1.0 \text{ nm}$ ) when the cross-linking was performed for 20 min, indicating a low degree of swelling.

**pH Response of  $(\text{PMAA}-\text{co}-\text{NH}_2)_5$  Microcapsules.** Below the critical pH point of PMAA related to deprotonation of carboxylic groups, the capsule thickness was in the range of 22.6–24.0 nm (Figure 5). Increasing pH resulted in a gradual increase in the capsule thickness to  $44.1 \pm 5.1 \text{ nm}$  at pH 6.0 followed by a sharp drop to around 3 nm above pH 6.5. The same trend was observed for the surface microroughness: at pH values below the  $\text{p}K_a$  of PMMA, the microroughness was in the range of 2.7–3.9 nm, then reached its maximum of 6.2 nm at pH 6.0, and finally decreased to less than 2.0 nm above pH 6.5 (Figure 5). Above pH 6.5, capsules exhibit sharp volume phase transition caused by deprotonation of carboxylic groups, resulting in dramatic decrease in the shell thickness.<sup>59,60</sup> As a result, increased buildup of osmotic pressure results in disruption of shells under these conditions (Figure 5).

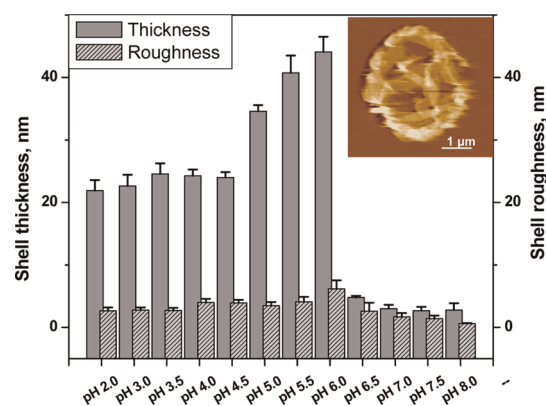


**Figure 5.** Thickness and microroughness of cross-linked ( $(\text{PMAA}-\text{co}-\text{NH}_2)_5$ ) capsules for 40 min in the swollen state at a wide pH range. Inset shows distorted capsule during AFM scanning at pH 7.0. Data shown are the average with standard deviation ( $n = 15$ ).

Sharp changes in the surface charges and volume transitions in different types of solvents (nanopure water and SMM media) were confirmed with CLSM and  $\zeta$ -potential measurements (Figure 6). The highest amplitude of charge changes was observed in pure water when  $\zeta$ -potential was gradually dropping from a positive value ( $+12 \pm 1.6 \text{ mV}$  at pH 3.0) to a negative value ( $-68 \pm 1.2 \text{ mV}$  at pH 6.5) (Figure 6a). Although in cell media capsules went through similar charge changes, the amplitude of such changes was less pronounced: from  $+4.8 \pm 0.4 \text{ mV}$  at pH 3.0 to  $-25.2 \pm 1.3 \text{ mV}$  at pH 7.5 (Figure 6b). Smaller change in  $\zeta$ -potential amplitude can be associated with larger molecules present in the media (amino acids) that are trapped within the polymer loops.<sup>47</sup> Hence, there is a significant ionic screening of the electrostatic repulsions between charges of equal sign.<sup>61</sup>

Confocal images of hollow cross-linked ( $(\text{PMAA}-\text{co}-\text{NH}_2)_5$ ) capsules showed dramatic changes in the capsule diameter which accompanies changes in the surface charges discussed above (Figure 6). Below pH 5.0, hollow capsules of  $3.4 \pm 0.5 \mu\text{m}$  diameter were close to the size of original silica templates. Above pH 5.0, capsules began to swell and reached their maximum swelling at pH 7.5 with capsule diameter of  $10.5 \pm 0.2 \mu\text{m}$  in the case of pure water and  $9.6 \pm 0.4 \mu\text{m}$  in SMM media (Figures 6 and 7). It is important to note that all dimensional changes are completely reversible during multiple cycling between low and high pH values (Figure 7).

The studies of localized mechanical properties of capsules using surface force spectroscopy (SFS) have revealed distinct changes in the capsule elasticity as a function of pH (Figure 8). The loading curves followed Hertzian contact mechanics, thus indicating elastic deformation of shells under probing conditions (Figure 8a). Overall, capsules with the largest molecular weight of PVPON were about 25% stiffer (Supporting Information, Figure S1). At 20 min of cross-linking time, the elastic modulus of shells was measured to be

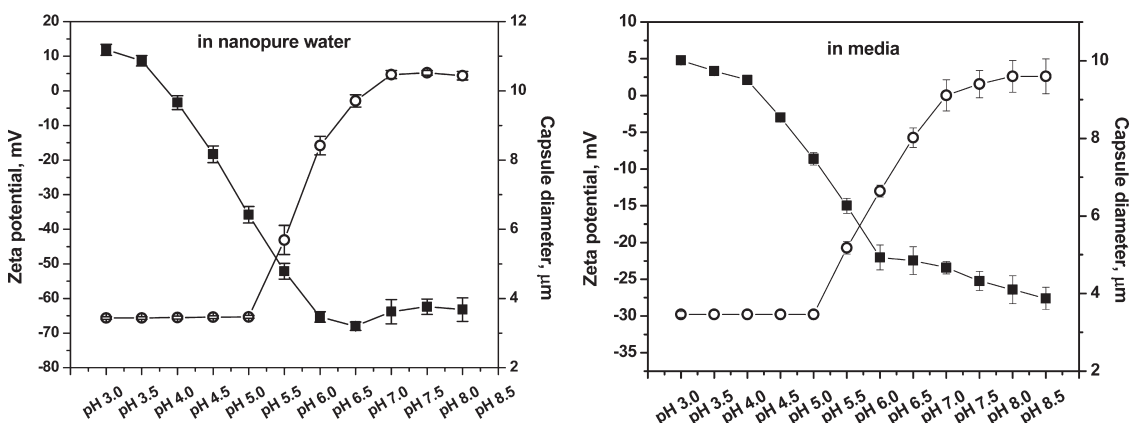


Figure 6. Zeta-potential (filled squares) and diameter (circles) of hollow cross-linked (PMAA-co-NH<sub>2</sub>)<sub>5</sub> capsule in different solutions at different pH values. Data shown are the average with standard deviation ( $n = 3$  for  $\zeta$  values,  $n = 10$  for diameter size).

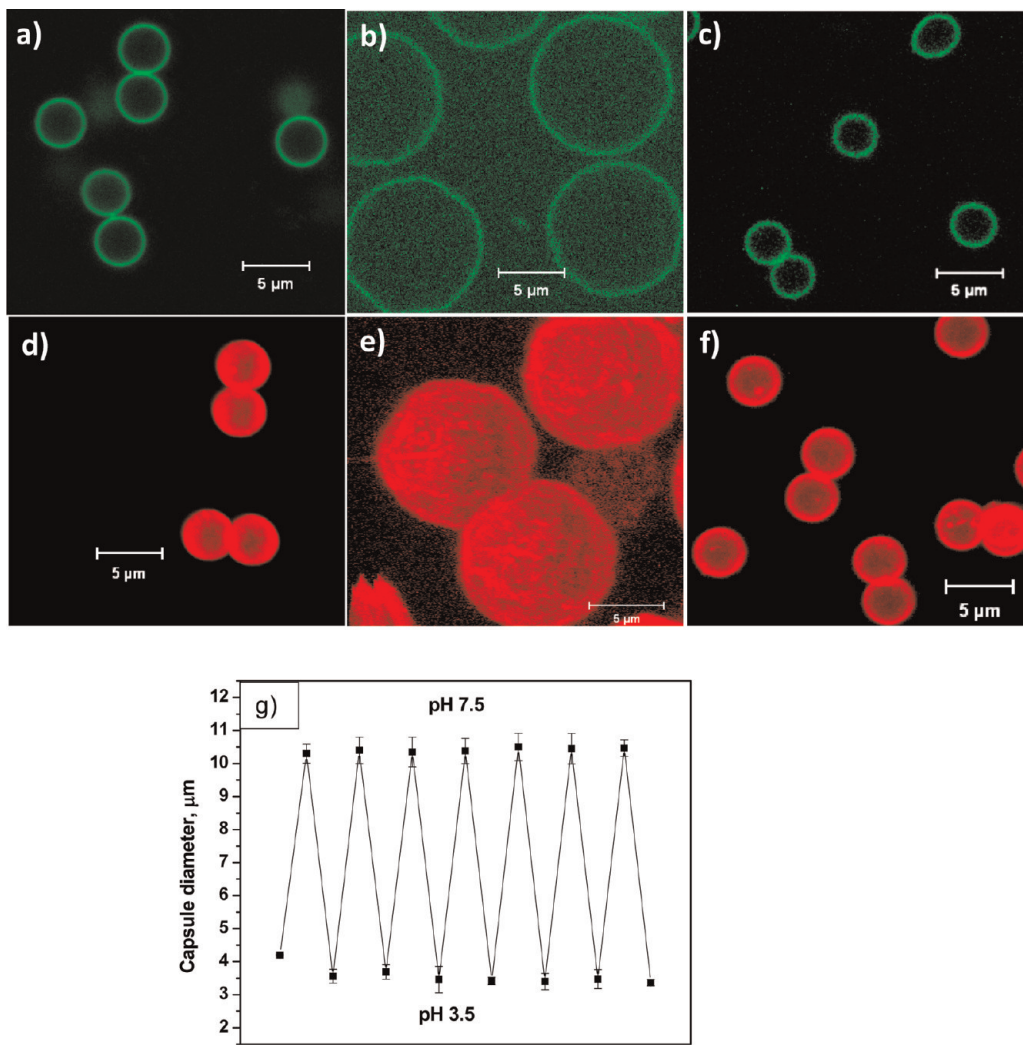
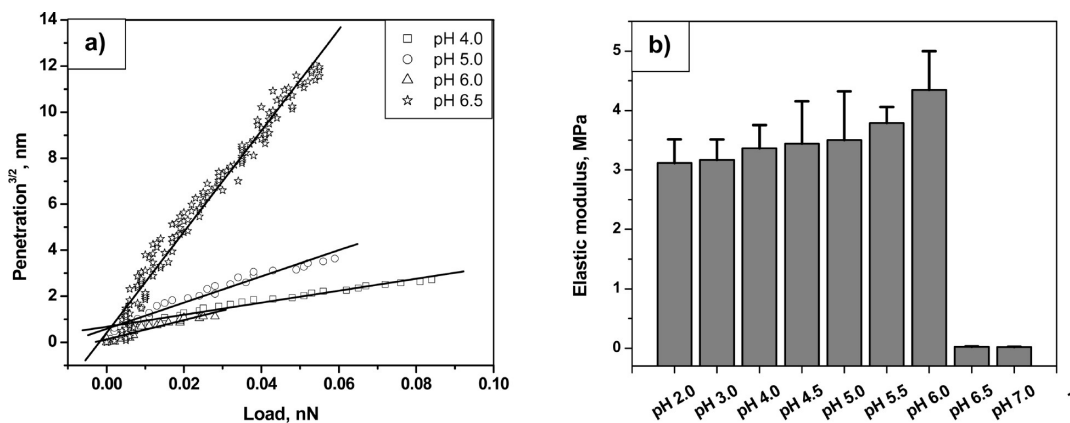


Figure 7. Cross section (top row) and reconstructed 3D (bottom row) confocal images of (PMAA-co-NH<sub>2</sub>)<sub>5</sub> capsules in aqueous solution initially at pH 3.0 (a,d), then at elevated pH 8.0 (b,e), and finally switched back to pH 3.0 (c,f). Reversible swelling/shrinking of (PMAA-co-NH<sub>2</sub>)<sub>5</sub> capsules at pH 3.5 and 7.5 (g). Data shown are the average with standard deviation ( $n = 10$ ).

$0.76 \pm 0.13$  MPa, and the value consequently increased, 4-fold, up to  $3.1 \pm 0.4$  MPa for the highest cross-linking density at 40 min (Figure 8b). While non-cross-linked capsules above pH 6.0 were readily

disassociated, cross-linked capsules were robust enough to undergo reversible swelling even at pH >7.

The range of Young's modulus of 3.2–4.3 MPa at low pH obtained here is typical for partially swollen



**Figure 8.** Loading curves for swollen capsules at different pH values in Hertzian coordinates (a). Elastic modulus of swollen ( $(\text{PMAA}-\text{co}-\text{NH}_2)_5$ ) microcapsules cross-linked for 40 min as a function of pH (b). Data shown are the average with standard deviation ( $n = 7$ ).

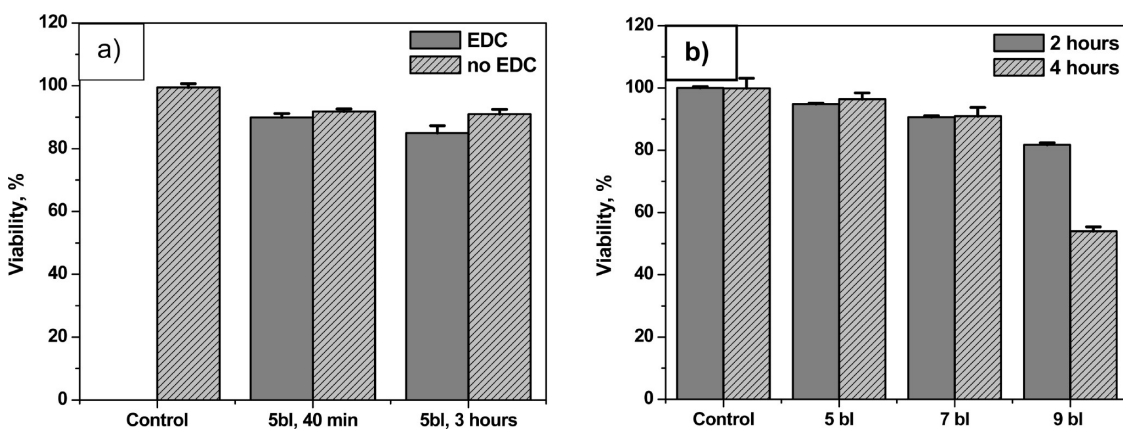


**Figure 9.** Cell viability of nontreated YPH501 (control) yeast cells in comparison to ( $(\text{PMAA}-\text{co}-\text{NH}_2)_5$ )-coated cells that were treated with EDC for 40 min (5bl-EDC, 40 min) and 3 h (5bl-EDC, 3 h) (a). Cell viability of nontreated yeast cells and coated with different composition of layers (5, 7, and 9 bilayers) after 2 and 4 h incubation with resazurin assay (b). Data shown are the average with standard deviation ( $n = 300$ ).

hydrogel elastomers.<sup>62–64</sup> With increasing pH of the solution above  $\text{p}K_a$ , the elastic modulus decreases by 2 orders of magnitude to about 20 kPa, which is a characteristic of a weakly cross-linked and highly swollen hydrogel material.<sup>65</sup> Decreased stiffness of the cross-linked ( $(\text{PMAA}-\text{co}-\text{NH}_2)_5$ ) capsules correlates well with remarkable swelling within the same range of pH 5.5–6.5 and provides means for dramatic stretching of thin shells (Figures 6 and 9). We suggest that such softening is caused by deprotonation of the acidic groups and repulsive charge–charge interactions.

Capsule softening within the narrow pH range was also reported for (PVPOON-*co*-NH<sub>2</sub>/PMAA) capsules by Fery *et al.*<sup>66</sup> Young's modulus of these two-component capsules at pH 2.0, however, was estimated to be much higher ( $610 \pm 70$  MPa), likely due to a much higher cross-linking density and low solvation of shells. This value is common for highly cross-linked elastomeric materials with low residual solvent.<sup>67</sup> In their study, the elastic modulus for higher pH was suggested to be around 1 MPa, but the actual value cannot be directly

measured with colloidal probe loading of capsules. In contrast, the SFS employed here probes local nanoscale properties under very light normal forces (80 pN) and small deformations (below 10 nm). It can also be employed even if the partial disassembly of capsules began to occur by finding intact planar areas.

Overall, dramatic changes observed here in the shell thickness, microroughness, and elasticity at the  $\text{p}K_a$  of PMAA copolymer can all be associated with increased deprotonation of unbound PMAA-*co*-NH<sub>2</sub> carboxylic groups when Coulombic interactions cause electrostatic repulsion produced within the network.<sup>25,50,54</sup> At  $\text{p}K_a$ , dissociation of unbound carboxylic groups on the network chains increases the charge density on the network to the highest degree. The increase in mobile counterion content increases the internal osmotic pressure, which induces the swelling of the hydrogel until the network chains reach a maximum of ionization and maximizes the capsule diameter. Overall, swelling in a wide pH range seems to occur in two stages: (1) at the acidic conditions

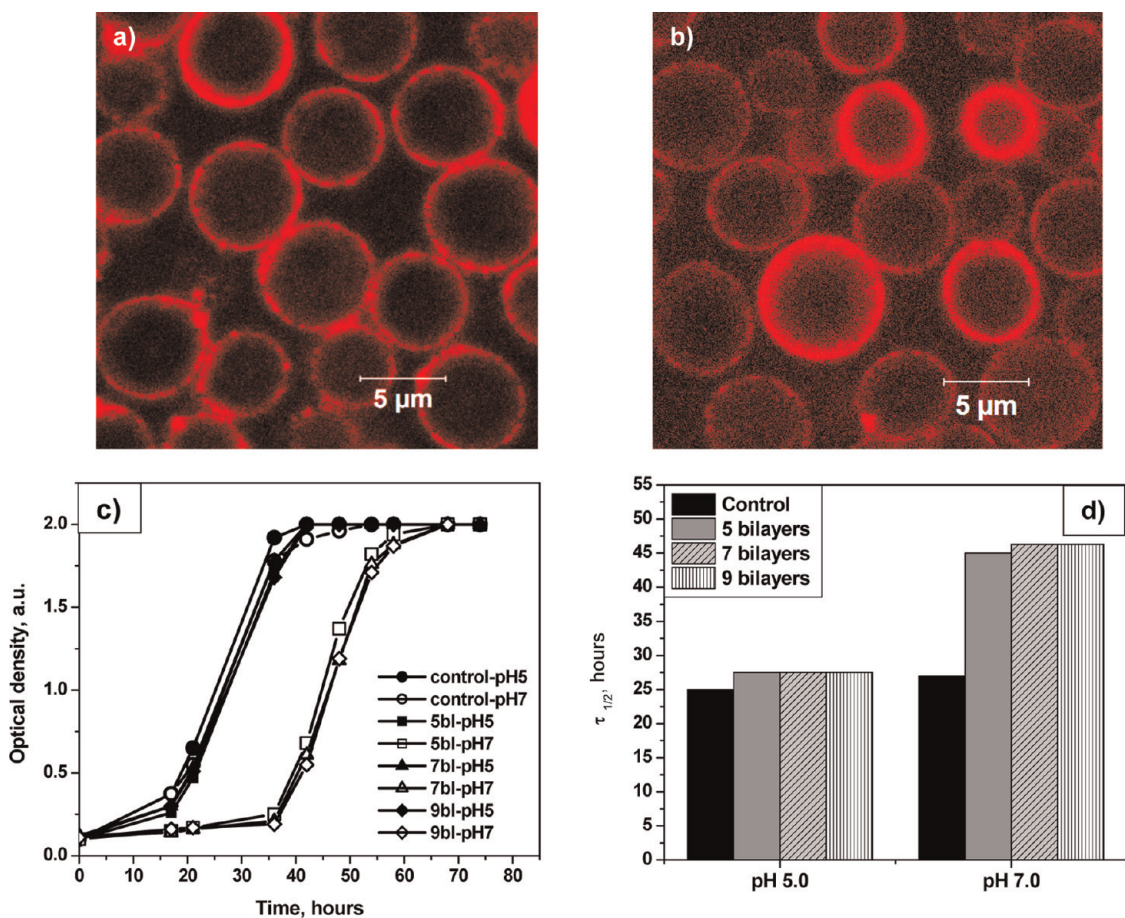


**Figure 10.** (PMAA-co-NH<sub>2</sub>)<sub>9</sub>-coated yeast cells at pH 5.0 (a) and pH 7.0 (b). Growth kinetics of (PMAA-co-NH<sub>2</sub>)-coated yeast cells with different shell thicknesses. Cells were grown in SMM media adjusted to pH 5.0 and 7.0 (c); 50% growth time for bare and encapsulated cells at pH 5.0 and 7.0 (d).

(pH 3.0–5.5), PMAA shells are modestly swollen, uniform, and stiffer due to limited uptake of water molecules into partially hydrophobic shells; and (2) exponential increase in capsule diameter (more than 3-fold) and decrease in shell thickness and stiffness occurring above pH 5.5 all are due to the increased ionization of PMAA segments, which results in lateral stretching limited by cross-linking sites. Finally, at pH >7.0, partial disintegration of capsules begins to occur, which progresses at even higher pH values.

**Cells Encapsulated with pH-Responsive Shells.** High cell viability after encapsulation was a characteristic feature of all shells studied here (Figure 9). Surprisingly, *S. cerevisiae* yeast cells coated with PMAA-co-NH<sub>2</sub> shells and treated with EDC for different time periods showed excellent viability despite the presence of highly reactive cross-linking agent. As evidenced from the live-dead staining test, the cell viability rate was in the range of 90 ± 1.3% for cells treated with EDC for 40 min and slightly decreased to 85 ± 2.4% when the time of exposure to EDC was increased up to 3 h. With an increasing number of layers, hence increasing thickness of the shell, the viability of cells only slightly decreased to 82% for 9 bilayer shells.

The viability observed here is very high compared to common LbL encapsulation with the presence of cationic components. The toxicity of cationic components of traditional LbL shells toward a variety of cell types has been well-documented and mainly associated with charge reversal at cell membranes upon contact.<sup>68,69</sup> We suggest that very low cytotoxicity of (PMAA-co-NH<sub>2</sub>) shells fabricated here arises from the nature of intermolecular bonding in hydrogen-bonded shells and highly permeable network morphology after removal of the PVPPON component.<sup>39</sup> Indeed, shells fabricated in this study contain a very low fraction (several vol %) of amine groups. In order to evaluate surface potential during cell encapsulation, we performed ζ-potential measurements after deposition of each layer (Supporting Information, Figure S3). As confirmed by these measurements, initial negative charge of the cell membrane (−28.5 mV) was partially neutralized to −9.9 mV after deposition of neutral polymer (PVPPON) and oscillated within −10 to −13 mV, in contrast to drastic positive–negative variations in conventional polyelectrolyte membranes, thus suggesting minor presence of the cationic component.<sup>70</sup>

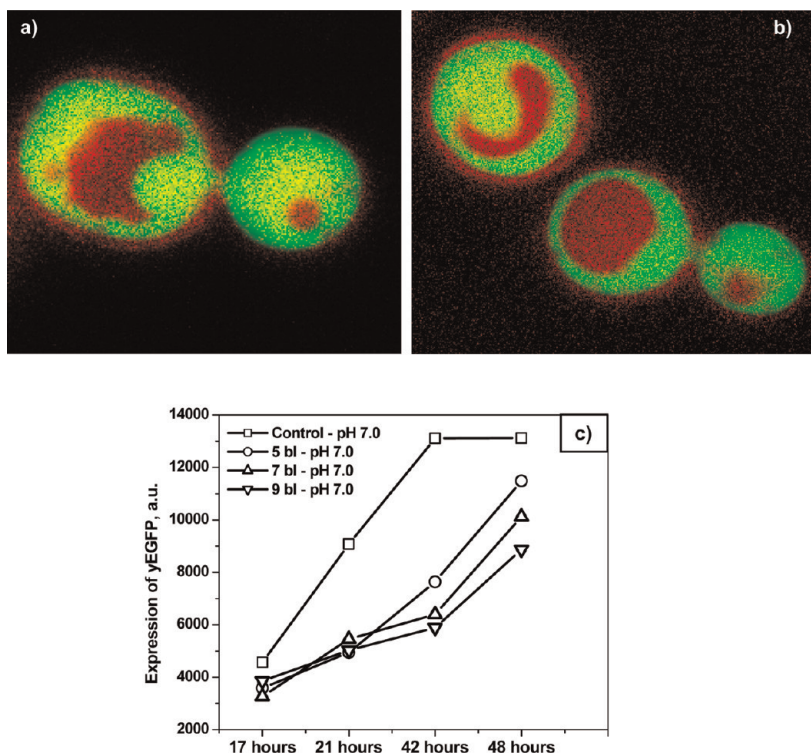


**Figure 11.** Expression of yEGFP 17 h after induction with 2% galactose. Cells were coated with (PMAA-co-NH<sub>2</sub>)<sub>7</sub> and grown in media at pH 5.0 (a) and pH 7 (b). Kinetics of yEGFP expression at different time points for cells grown at pH 7.0 (c).

The interesting novel feature observed in this study is the significant effect of the pH-responsive behavior of LbL shells on the cell growth and function. To test this behavior, bare and coated cells were introduced to a buffer solution at pH 5.0 and continuously monitored in a confocal microscope while the pH of the solution gradually increased (Figure 10). In this experiment, we observed that, even at pH 9.0, the shells (labeled with dye) stayed intact and permanently attached to the cells without any indication of dramatic swelling, which was observed for hollow capsules (Figure 7). We suggest that strong attachment of the LbL shell to the cell wall is facilitated by the multiple ionic interactions, hydrogen bonding, and chemical cross-linking.<sup>71–73</sup> Since cell walls are rich in amine-bearing ligands, strong tethering between polymer shells and cell walls can easily occur during an incubation period with a cross-linking agent.

However, a dramatic effect of pH was observed in the growth behavior of bare and encapsulated shells when cells were grown in two separate flasks with SMM media adjusted to pH 5.0 and 7.0 (Figure 10). The formation of budded daughter cells and expression of yeast-enhanced green fluorescent protein (yEGFP) were monitored until the stationary phase had reached its plateau at 48 h for pH 5.0 and 72 h for pH 7.0. As observed, the growth of bare cells was not affected by pH with the half-time of the growth cycle close to 25 h in both cases. In contrast, all encapsulated cells showed dramatic change in a growth mode at pH 7. In all cases

for encapsulated cells with different shell thickness, budding and replication were delayed by about 24 h with half-time growth close to 47 h (Figure 10). Additional independent studies confirmed tolerance of bare *S. cerevisiae* yeast cells to alkali conditions with growth behavior and expression rate of yEGFP remaining intact (Supporting Information, Figure S3). Strong fluorescence coming from yEGFP expression was observed when cells were grown in the presence of 2% galactose at both pH 5.0 and 7.0 with hydrogel shell still present after 17 h of yEGFP induction (Figure 11).

Such a strong effect of the presence of (PMAA-co-NH<sub>2</sub>) shells on the function of encapsulated cells at higher pH can be associated with pH-triggered changes in the state of free carboxylate groups and shell thickness. Progressive deprotonation above pH 5.0 increases the degree of ionization and drives surface potential to increased net negative charge (Figure 6). Increased thickness of the shells at pH 7.0 should result in a reduced transport of nutrients, thus delaying the cell growth. Indeed, in our recent study of hydrogen-bonded shells, we observed dramatic, many-fold reduction of the transport across shells with increasing thickness.<sup>39,40</sup>

## CONCLUSIONS

In conclusion, we demonstrated the high biocompatibility of newly fabricated pH-responsive cross-linked PMMA hydrogel shells. Low cross-linking density of hydrogel PMAA-co-NH<sub>2</sub> shells resulted in

unaltered growth kinetics of encapsulated cells at pH below 5.5 with excellent viability reaching 90%. The formation of pH-sensitive LbL shells directly on the cell surfaces allowed the control of cell growth by variation in pH without affecting cell function as indicated by stable *y*EGFP expression. By keeping encapsulated cells at physiologically relevant conditions (pH 7.0), we were able to postpone the replication process without inhibition of biosensing activity (induced GFP generation) of the cells. The ability to manipulate perceptible response from the cells by keeping them in

"dormant" conditions (constrained replication) for the extended time can be rewarding for biosensing applications when the early onset of cell growth can compromise the long-term performance. In this sense, our pH-responsive LbL shells behave as an active barrier that controls the growth behavior and the function of cells. Considering the fact that PMAA-*co*-NH<sub>2</sub> shells were pH-responsive at physiologically relevant conditions required for normal biological functions, they might find significant interest for both *in vitro* and *in vivo* biological applications.

## MATERIALS AND METHODS

**Materials.** Poly(*N*-vinylpyrrolidone) (55 and 1300 kDa) (PVPON55, PVPON1,300), a monomer of methacrylic acid (MAA), hydrochloric acid, sodium hydroxide, sodium chloride, monobasic sodium phosphate, and 1-ethyl-3-(dimethylamino-propyl)carbodiimide hydrochloride (EDC) were purchased from Sigma-Aldrich. Initiator, 2,2'-azobis(2-methylpropionitrile) (AIBN), was purchased from Sigma-Aldrich and recrystallized from methanol at 30 °C before use. Poly(methacrylic acid) (100 kDa) (PMAA), a monomer, *N*-(*t*-tert-butoxycarbonylaminopropyl)methacrylamide (*t*-BOCAPMA) for synthesis of amine-functionalized PMAA, and 4.0 ± 0.2 μm silica particles as 10% aqueous suspension were purchased from Polysciences Inc. Hydrofluoric acid (HF) (48–51%) was purchased from BDH Aristar. All chemicals were used without further purification. Nanopure (Barnstead Nanopure system) water with a resistivity of 18.2 MΩ·cm was used in all experiments.

The *S. cerevisiae* YPH501 diploid yeast strain expressing a plasmid encoding yeast-enhanced green fluorescent protein as a biomarker was used for this study.<sup>39</sup> Cells were cultured in synthetic minimal medium (SMM) supplemented with 2% raffinose solution. Yeast cells were grown at 30 °C in a shaker incubator (New Brunswick Scientific) with 220 rpm to bring them to an early exponential phase when optical density reached 0.4–0.5 au based on a 0–2 scale (absorbance was measured at 600 nm on a GE cell calculator).

Cell viability was assessed immediately after encapsulation process with live–dead and rezasurin assay kits according to manufacturer's protocols (BioVision).<sup>74</sup> For live–dead test, representative images were collected with Zeiss 510 Vis LSM using a band-pass filter (ex/em = 488/515 and 543/560 nm for detection of FITC and rhodamine, respectively). Confocal micrographs were analyzed with Zen2009 software to quantify the number of pixels corresponding to fluorescent emission from live (green) and dead (red) cells. For rezasurin-based assay, fluorescence was measured at 585 nm (ex = 560 nm) on a spectrofluorophotometer (Shimadzu RF 5301 PC) after incubation for 2 and 4 h.

**Synthesis of Amino-Containing Copolymer of Methacrylic Acid, PMAA-*co*-NH<sub>2</sub>.** PMAA-*co*-NH<sub>2</sub> copolymer was synthesized using bulk copolymerization of MAA and *t*-BOCAPMA. For PMAA-*co*-NH-BOC synthesis, 8.7 mL (100 mmol) of MAA and 658 mg (2.9 mmol) of *t*-BOCAPMA were mixed in a round-bottom flask. The solution was deoxygenated by bubbling with nitrogen for 30 min. After that, the mixture was heated to 45 °C and stirred. Then, 40 mg (0.25 mmol) of AIBN was added to the flask, and the reaction mixture was stirred under nitrogen atmosphere for 3 h. The reaction was terminated after 3 h by pouring the mixture into a 10-fold excess volume of diethyl ether. The precipitated copolymer was dissolved in tetrahydrofuran and precipitated in hexane. After a repeated precipitation step, the copolymer was dried in vacuum. *t*-Boc protecting groups were hydrolyzed by treating the copolymer with 1 M HCl in methanol for 100 h. Solutions of the deprotected copolymers were dialyzed against nanopure water using a Slide-A-Lyzer dialysis cassette (Thermo Scientific) with a molecular weight cutoff of 10 kDa and lyophilized.

Composition of the resultant amino-containing copolymer prior and/or after hydrolysis of Boc protective groups was determined by using NMR (Bruker DSX 400). The change in integral intensity in the spectrum of protected PMAA-*co*-NH-BOC in comparison with that of deprotected PMAA-*co*-NH<sub>2</sub>, due to hydrolysis of *t*-Boc groups, allowed calculation of the percentage of amino groups in the copolymer.<sup>75</sup> NMR analysis shows that the copolymer contained 17% of amine groups (data not shown). The molecular weight of PMAA-*co*-NH<sub>2</sub> was determined using GPC (Waters, 717 plus) equipped with a HPLC pump (Waters, 1515) at flow rate of 1 mL/min in THF at 25 °C and three columns (guard and two PLgel 5 μm MIXED-C columns). A calibration curve based on PS standards was used in conjunction with a differential refractive index detector (Waters, 2414). The *M*<sub>w</sub> of the resultant amino-containing copolymer was determined to be 14 kDa (PDI = 1.4).

**Encapsulation of Yeast Cells with Cross-Linked (PMAA-*co*-NH<sub>2</sub>) Shells.** LbL assembly was employed for encapsulation of individual yeast cells based on hydrogen-bonded interactions between PVPON and PMAA-*co*-NH<sub>2</sub> components. Before deposition of (PVPON/PMAA-*co*-NH<sub>2</sub>)<sub>n</sub> LbL shells (where *n* denotes number of bilayers), yeast cells were harvested in 2 mL centrifuge tubes and washed three times with phosphate buffer (0.01 M, pH 5). PVPON and PMAA-*co*-NH<sub>2</sub> were assembled onto cell walls from 0.5 mg/mL aqueous solutions (0.01 M phosphate buffer, pH 3.5) for 15 min. Cross-linking was performed for 40 min using EDC (5 mg/mL, 0.01 M phosphate buffer, pH 5.0). During deposition and cross-linking, cells were redispersed by gentle rotation at 60 rpm at ambient conditions. After each deposition step, cells were collected into the pellet by centrifugation at 2000 rpm for 2 min and washed two times with phosphate buffer (0.01 M, pH 3.5) to remove the PVPON layer and residual cross-linking agent.

**Preparation of Cross-Linked (PMAA-*co*-NH<sub>2</sub>)<sub>n</sub> Capsules.** Capsules were prepared on silica cores using the same concentrations and buffer solutions according to the established procedure.<sup>55</sup> For comparison of mechanical stability, we also prepared non-cross-linked capsules, where 0.5 mg/mL of native PMAA and 0.5 mg/mL PVPON of different molecular weights, PVPON55K and PVPON1,300K, were prepared in 0.01 M phosphate buffer adjusted to pH 3.5. Hydrogen-bonded LbL shells were deposited on a sacrificial silica core starting from PVPON followed by PMAA-*co*-NH<sub>2</sub> until the desired thickness was achieved. The deposition time for each layer was 15 min under gentle shaking at 250 rpm using a vortex-shaker (VWR analog vortex). After each deposition, particles were centrifuged at 2000 rpm for 2 min and washed with 0.01 M phosphate buffer solution three times.

To prepare cross-linked capsules, silica particles with five polymer bilayers were introduced into the solution of EDC (5 mg/mL, 0.01 M phosphate buffer at pH 5.0) for 20, 30, and 40 min with consecutive washing in phosphate buffer solution at pH 6.0 for at least 1 h to remove coupling agent, reaction byproducts, and the PVPON layer. Un-cross-linked PVPON component and silica material were removed and dissolved in 8% aqueous hydrofluoric acid (HF) for 4 h with gentle shaking in the vortex to remove the sacrificial template and release hollow

capsules. Exhaustive dialysis against nanopure water adjusted to pH 3.5 was performed for the next 72 h to remove any traces of HF. Dialysis of hydrogel capsules was performed in 1 mL Float-A-Lyzer dialyzing cassettes with 20 kDa cutoff pore size cellulose ester membranes.

**Characterization.** ATR-FTIR measurements of hollow PMAA-co-NH<sub>2</sub> capsules before and after cross-linking with EDC were performed on a Bruker FTIR spectrometer Vertex 70.<sup>76</sup> Spectra were collected at 4 cm<sup>-1</sup> resolution, and the number of scans was 120. Aqueous solutions of capsules were spin-coated on ATR crystal for 30 s (rpm = 3000).

Surface morphology of the hollow capsules in dry and swollen states was examined with AFM according to the established procedure.<sup>77,80</sup> The topographical and phase images were collected with a Dimension-3000 AFM (Digital Instruments) in light tapping mode using silicon V-shape cantilevers having a spring constant of 46 N/m for dry capsules and 0.046 N/m for swollen capsules using a liquid cell.<sup>78</sup> AFM nanomechanical measurements of capsules in the swollen state were performed separately at different pH values by collecting 16 × 16 point arrays of force–distance curves for at least 5–6 capsules to ensure representative results.<sup>79,80</sup> Prior to scanning in liquid, capsules were air-dried from aqueous solution at pH 3.5 and scanned in nanopure water adjusted to specified pH values. The spring constants of the cantilevers were determined by their thermal resonance frequency spectra. The tip radius was estimated by scanning 5 nm gold nanoparticle standards and performing deconvolution calculation using custom-made MMA processing software.<sup>80</sup> Data processing and evaluation of the adhesion distribution were performed using the Sneddon's model.<sup>81</sup> The indentation depth was limited to 2–10 nm to avoid plastic deformation.

Scanning electron microscopy (SEM) imaging of hollow capsules was performed on Hitachi S-3400-II electron microscope at 10 kV in low vacuum regime. Before imaging, capsules were air-dried on silicon wafers and sputter-coated with gold. Surface potentials of cross-linked hollow capsules at pH values starting from pH 3 up to pH 8.5 were measured in 0.01 M phosphate buffer and SMM media solutions on Zetasizer Nano-ZS equipment (Malvern). Each value of zeta-potential was obtained at ambient conditions by averaging three independent measurements of 35 subruns each.

Confocal laser scanning microscopy (CLSM) images of yeast cells encapsulated with different shells and hollow capsules were obtained on LSM 510 UV-vis inverted laser scanning microscope equipped with 63 × 1.4 oil immersion objective lens (Zeiss). To visualize the shell around cells, PMAA-co-Alexa568 was deposited as a top layer (2 mg/mL, 0.01 M phosphate buffer, pH 4.5). For detailed procedure on the synthesis of fluorescently labeled PMAA-co-Alexa568, refer to our previous paper.<sup>39</sup> For colocalization of shell and fluorescence coming from yEGFP, encapsulated cells were incubated in 2% galactose at 30 °C to induce yEGFP expression. Cells were visualized by consecutive scanning mode using two filters with excitation/emission wavelengths 488/515 nm for detection of yEGFP and 543/560 nm for detection of PMAA-co-Alexa568. Hollow capsules were visualized by adding FITC solution (1 mg/mL in 0.01 M phosphate buffer, pH 3.5) to the aqueous suspension of capsules in Lab-Tek chambers (Electron Microscopy Sciences). Excitation/emission wavelength was 488/515 nm for detection of FITC.

To study the pH-responsive coating on cells, we prepared two separate SMM solutions adjusted to pH 5.0 and 7.0. Coated cells with different shell thickness were allowed to grow until the stationary phase was reached. We also tested capsules in nanopure water and SMM media at pH 3.0–8.0. The effect of pH on capsule's size was observable within 15–30 s after change in the ionic strength. Three-dimensional reconstructed images were obtained using fluorescently labeled PMAA (PMAA-co-Alexa532).<sup>39</sup>

**Conflict of Interest:** The authors declare no competing financial interest.

**Acknowledgment.** The study is supported by Grants FA9550-11-1-0233 and FA9550-09-1-0162 (BIONIC Center) from

Air Force Office of Scientific Research (cell encapsulation) and Project # DE-FG02-09ER46604 from Department of Energy (DOE) (shell formation). We are grateful to Prof. N. Kroger for providing access to Zeta-sizer, and S. Young for the help with ATR-FTIR.

**Supporting Information Available:** Detailed calculations of  $M_c$ , molecular weight between the cross-linking points, mesh size of hydrogel, and Figures S1–S3. This material is available free of charge via the Internet at <http://pubs.acs.org>.

## REFERENCES AND NOTES

- Liu, F.; Urban, M. W. Recent Advances and Challenges in Designing Stimuli-Responsive Polymers. *Prog. Polym. Sci.* **2010**, *35*, 3–23.
- Cole, M. A.; Voelcker, N. H.; Thissen, H.; Griesser, H. Stimuli-Responsive Interfaces and Systems for the Control of Protein–Surface and Cell–Surface Interactions. *Biomaterials* **2009**, *30*, 1827–1850.
- De Las Heras Alarcon, C.; Pennadam, S.; Alexander, C. Stimuli Responsive Polymers for Biomedical Applications. *Chem. Soc. Rev.* **2005**, *34*, 276–285.
- Stevens, M. M.; George, J. H. Exploring and Engineering the Cell Surface Interface. *Science* **2005**, *310*, 1135–1138.
- Langer, R.; Peppas, N. A. Advances in Biomaterials, Drug Delivery, and Bionanotechnology. *AIChEJ* **2003**, *49*, 2990–3006.
- Cohen Stuart, M. A.; Huck, W. T. S.; Genzer, J.; Müller, M.; Ober, Ch.; Stamm, M.; Sukhorukov, G. B.; Szleifer, I.; Tsukruk, V. V.; Urban, M.; Winnik, F.; et al. Emerging Applications of Stimuli-Responsive Polymer Materials. *Nat. Mater.* **2010**, *9*, 101–113.
- Luzinov, I.; Minko, S.; Tsukruk, V. V. Adaptive and Responsive Surfaces through Controlled Reorganization of Interfacial Polymer Layers. *Prog. Polym. Sci.* **2004**, *29*, 635–698.
- Ebara, M.; Yamato, M.; Hirose, M.; Aoyagi, T.; Kikuchi, A.; Sakai, K.; Okano, T. Copolymerization of 2-Carboxyisopropylacrylamide with N-Isopropylacrylamide Accelerates Cell Detachment from Grafted Surfaces by Reducing Temperature. *Biomacromolecules* **2003**, *4*, 344–349.
- Ecckman, F.; Moes, A. J.; Amighi, K. Synthesis and Characterization of Thermosensitive Copolymers for Oral Controlled Drug Delivery. *Eur. Polym. J.* **2004**, *40*, 873–881.
- Vihola, H.; Laukkonen, A.; Valtola, L.; Tenhu, H.; Hirvonen, J. Cytotoxicity of Thermosensitive Polymers Poly(N-isopropylacrylamide), Poly(N-vinylcaprolactam) and Amphiphilically Modified Poly(N-vinylcaprolactam). *Biomaterials* **2005**, *26*, 3055–3064.
- Zhu, Z.; Sukhishvili, S. A. Temperature-Induced Swelling and Small Molecule Release with Hydrogen-Bonded Multilayers of Block Copolymer Micelles. *ACS Nano* **2009**, *3*, 3595–3605.
- Yamato, M.; Kwon, O. H.; Hirose, M.; Kikuchi, A.; Okano, T. Novel Patterned Cell Coculture Utilizing Thermally Responsive Grafted Polymer Surfaces. *J. Biomed. Mater. Res.* **2001**, *55*, 137–140.
- Uchida, K.; Sakai, K.; Ito, E.; Kwon, O. H.; Kikuchi, A.; Yamato, M.; Okano, T. Temperature-Dependent Modulation of Blood Platelet Movement and Morphology on Poly(N-isopropylacrylamide)-Grafted Surfaces. *Biomaterials* **2000**, *21*, 923–929.
- Connal, L. A.; Li, Q.; Quinn, J. F.; Tjipto, E.; Caruso, F.; Qiao, G. G. pH-Responsive Poly(acrylic acid) Core Cross-Linked Star Polymers: Morphology Transitions in Solution and Multilayer Thin Films. *Macromolecules* **2008**, *41*, 2620–2626.
- Becker, A. L.; Zelikin, A. N.; Johnston, A. P. R.; Caruso, F. Tuning the Formation and Degradation of Layer-by-Layer Assembled Polymer Hydrogel Microcapsules. *Langmuir* **2009**, *25*, 14079–14085.
- Murthy, N.; Campbell, J.; Fausto, N.; Hoffman, A. S.; Stayton, P. S. Bioinspired pH-Responsive Polymers for the Intracellular Delivery of Biomolecular Drugs. *Bioconjugate Chem.* **2003**, *14*, 412–419.

17. Gensel, J.; Borke, T.; Pérez, N. P.; Fery, A.; Andreeva, D. V.; Betthausen, E.; Müller, A. H. E.; Möhwald, H.; Skorb, E. V. Cavitation Engineered 3D Sponge Networks and Their Application in Active Surface Construction. *Adv. Mater.* **2012**, *24*, 985–989.
18. Zhu, X.; DeGraaf, J.; Winnik, F. M.; Leckband, D. pH-Dependent Mucoadhesion of a Poly(*N*-isopropylacrylamide) Copolymer Reveals Design Rules for Drug Delivery. *Langmuir* **2004**, *20*, 10648–10656.
19. Minko, S.; Müller, M.; Motornov, M.; Nitschke, M.; Grundke, K.; Stamm, M. Two-Level Structured Self-Adaptive Surfaces with Reversibly Tunable Properties. *J. Am. Chem. Soc.* **2003**, *125*, 3896–3900.
20. Cellesi, F.; Tirelli, N.; Hubbell, J. A. Towards a Fully-Synthetic Substitute of Alginate: Development of a New Process Using Thermal Gelation and Chemical Cross-Linking. *Biomaterials* **2004**, *25*, 5115–5124.
21. Kamath, K. P.; Park, K. Biodegradable Hydrogels in Drug Delivery. *Adv. Drug Delivery Rev.* **1993**, *11*, 59–84.
22. Schlenoff, J. B.; Decher, G. *Multilayer Thin Films: Sequential Assembly of Nanocomposite Materials*; Wiley-VCH: Weinheim, Germany, 2003.
23. Ruiz-Hitzky, E.; Ariga, K.; Lvov, Y. *Bio-inorganic Hybrid Nanomaterials: Strategies, Syntheses, Characterization and Applications*; Wiley-VCH: Weinheim, Germany, 2008.
24. Sukhishvili, S. A. Responsive Polymer Films and Capsules via Layer-by-Layer Assembly. *Curr. Opin. Colloid Interface Sci.* **2005**, *10*, 37–44.
25. Skirtach, A. G.; Yashchenok, A. M.; Möhwald, H. Encapsulation, Release and Applications of LbL Polyelectrolyte Multilayer Capsules. *Chem. Commun.* **2011**, *47*, 12736–12746.
26. Delcea, M.; Möhwald, H.; Skirtach, A. Stimuli-Responsive LbL Capsules and Nanoshells for Drug Delivery. *Adv. Polym. Sci.* **2011**, *63*, 730–747.
27. Kozlovskaya, V.; Kharlampieva, E.; Chang, S.; Muhlbauer, R.; Tsukruk, V. V. pH-Responsive Layered Hydrogel Microcapsules as Gold Nanoreactors. *Chem. Mater.* **2009**, *21*, 2158–2167.
28. Kozlovskaya, V.; Kharlampieva, E.; Khanal, B. P.; Manna, P.; Zubarev, E. R.; Tsukruk, V. V. Ultrathin Layer-by-Layer Hydrogels with Incorporated Gold Nanorods as pH-Sensitive Optical Materials. *Chem. Mater.* **2008**, *20*, 7474–7485.
29. Kharlampieva, E.; Kozlovskaya, V.; Zavgorodnya, O.; Lilly, G. D.; Kotov, N. A.; Tsukruk, V. V. pH-Responsive Photoluminescent LbL Hydrogels with Confined Quantum Dots. *Soft Matter* **2010**, *6*, 800–807.
30. Veerabadran, N. G.; Goli, P. L.; Stewart-Clark, S. S.; Lvov, Y. M.; Mills, D. K. Nanoencapsulation of Stem Cells within Polyelectrolyte Multilayer Shells. *Macromol. Biosci.* **2007**, *7*, 877–882.
31. Krol, S.; Nolte, M.; Diaspro, A.; Mazza, D.; Magrassi, R.; Gliozi, A.; Fery, A. Encapsulated Living Cells on Microstructured Surfaces. *Langmuir* **2005**, *21*, 705–709.
32. Franz, B.; Balkundi, S. S.; Dahl, C.; Lvov, Y. M.; Prange, A. Layer-by-Layer Nano Encapsulation of Microbes: Controlled Cell Surface Modification and Investigation of Substrate Uptake in Bacteria. *Macromol. Biosci.* **2010**, *10*, 164–172.
33. Diaspro, A.; Silvano, D.; Krol, S.; Cavalleri, O.; Gliozi, A. Single Living Cell Encapsulation in Nano-organized Polyelectrolyte Shells. *Langmuir* **2002**, *18*, 5047–5050.
34. Fakhruin, R. F.; Zamaleeva, A. I.; Morozov, M. V.; Tazetdinova, D. I.; Alimova, F. K.; Hilmutdinov, A. K.; Zhdanov, R. I.; Kahraman, M.; Culha, M. Living Fungi Cells Encapsulated in Polyelectrolyte Shells Doped with Metal Nanoparticles. *Langmuir* **2009**, *25*, 4628–4634.
35. Wilson, J. T.; Krishnamurthy, V. R.; Cui, W.; Qu, Z.; Chaikof, E. L. Noncovalent Cell Surface Engineering with Cationic Graft Copolymers. *J. Am. Chem. Soc.* **2009**, *131*, 18228–18229.
36. Becker, A. L.; Zelikin, A. N.; Johnston, A. P. R.; Caruso, F. Tuning the Formation and Degradation of Layer-by-Layer Assembled Polymer Hydrogel Microcapsules. *Langmuir* **2009**, *25*, 14079–14085.
37. Tiourina, O. P.; Radtchenko, I.; Sukhorukov, G. B.; Mohwald, H. Artificial Cell Based on Lipid Hollow Polyelectrolyte Microcapsules: Channel Reconstruction and Membrane Potential Measurement. *J. Membr. Biol.* **2002**, *190*, 9–16.
38. Wilson, J. T.; Cui, W.; Kozlovskaya, V.; Kharlampieva, E.; Pan, D.; Qu, Z.; Krishnamurthy, V. R.; Mets, J.; Kumar, V.; Wen, J.; et al. Cell Surface Engineering with Polyelectrolyte Multilayer Thin Films. *J. Am. Chem. Soc.* **2011**, *133*, 7054–7064.
39. Kozlovskaya, V.; Harbaugh, S.; Drachuk, I.; Shchepelina, O.; Kelly-Loughnane, N.; Stone, M.; Tsukruk, V. V. Hydrogen-Bonded LbL Shells for Living Cell Surface Engineering. *Soft Matter* **2011**, *7*, 2364–2372.
40. Carter, J. L.; Drachuk, I.; Harbaugh, S.; Kelley-Loughnane, N.; Stone, M.; Tsukruk, V. V. Truly Nonionic Polymer Shells for the Encapsulation of Living Cells. *Macromol. Biosci.* **2011**, *11*, 1244–1253.
41. Shchepelina, O.; Drachuk, I.; Gupta, M. K.; Lin, J.; Tsukruk, V. V. Silk-on-Silk Layer-by-Layer Microcapsules. *Adv. Mater.* **2011**, *23*, 4655–4660.
42. Ye, C.; Shchepelina, O.; Calabrese, R.; Drachuk, I.; Kaplan, D. L.; Tsukruk, V. V. Robust and Responsive Silk Ionomer Microcapsules. *Biomacromolecules* **2011**, *12*, 4319–4325.
43. Balkundi, S. S.; Veerabadran, N. G.; Eby, D. M.; Johnson, G. R.; Lvov, Y. M. Encapsulation of Bacterial Spores in Nanoorganized Polyelectrolyte Shells. *Langmuir* **2009**, *25*, 14011–14016.
44. Henry, A. C.; Tutt, T. J.; Galloway, M.; Davidson, Y. Y.; McWhorter, C. S.; Soper, S. A.; McCarley, R. L. Surface Modification of Poly(methyl methacrylate) Used in the Fabrication of Microanalytical Devices. *Anal. Chem.* **2000**, *72*, 5331–5337.
45. Venyaminov, S. Yu.; Kalinin, N. N. Quantitative IR Spectrophotometry of Peptide Compounds in Water ( $H_2O$ ) Solutions. I. Spectral Parameters of Amino Acid Residue Absorption Bands. *Biopolymers* **1990**, *30*, 1243–1257.
46. Sukhishvili, S. A.; Granick, S. Layered, Erasable Polymer Multilayers Formed by Hydrogen-Bonded Sequential Self-Assembly. *Macromolecules* **2002**, *35*, 30–310.
47. Kozlovskaya, V.; Yakovlev, S.; Libera, M.; Sukhishvili, S. A. Surface Priming and the Self-Assembly of Hydrogen-Bonded Multilayer Capsules and Films. *Macromolecules* **2005**, *38*, 4828–4836.
48. Chang, M. C.; Tanaka, J. FT-IR Study for Hydroxyapatite/Collagen Nanocomposite Cross-Linked by Glutaraldehyde. *Biomaterials* **2002**, *23*, 4811–4818.
49. Izumrudov, V. A.; Kharlampieva, E.; Sukhishvili, S. A. Multilayers of a Globular Protein and a Weak Polyacid: Role of Polyacid Ionization in Growth and Decomposition in Salt Solutions. *Biomacromolecules* **2005**, *6*, 1782–1788.
50. Kozlovskaya, V.; Sukhishvili, S. A. Amphoteric Hydrogel Capsules: Multiple Encapsulation and Release Routes. *Macromolecules* **2006**, *39*, 6191–6199.
51. Szarpak, A.; Cui, D.; Dubreuil, F.; De Geest, B. G.; De Cock, L. J.; Picart, C.; Auzely-Veltý, R. Designing Hyaluronic Acid-Based Layer-by-Layer Capsules as a Carrier for Intracellular Drug Delivery. *Biomacromolecules* **2010**, *11*, 713–720.
52. Moshnikova, A. B.; Afanasyev, V. N.; Proussakova, O. V.; Chernyshov, S.; Gogvadze, V.; Beletsky, I. P. Cytotoxic Activity of 1-Ethyl-3-(3-dimethylaminopropyl)-Carbodiimide Is Underlain by DNA Interchain Cross-Linking. *Cell. Mol. Life Sci.* **2006**, *63*, 229–234.
53. Brannion-Peppas, L.; Peppas, N. A. Equilibrium Swelling Behavior of pH-Sensitive Gels. *Chem. Eng. Sci.* **1991**, *3*, 715–722.
54. Bell, C.; Peppas, N. A. Water, Solute and Protein Diffusion in Physiologically Responsive Hydrogels of Poly(methacrylic acid-g-ethylene glycol). *J. Controlled Release* **1996**, *39*, 1203–1218.
55. Kozlovskaya, V.; Kharlampieva, E.; Drachuk, I.; Cheng, D.; Tsukruk, V. V. Responsive Microcapsule Reactors Based on Hydrogen-Bonded Tannic Acid Layer-by-Layer Assemblies. *Soft Matter* **2010**, *6*, 3596–3608.
56. Jiang, C.; Markusya, S.; Pikus, Y.; Tsukruk, V. V. Freely Suspended Nanocomposite Membranes as Highly Sensitive Sensors. *Nat. Mater.* **2004**, *3*, 721–728.

57. LeMieux, M. C.; Lin, Y.-H.; Cuong, P. D.; Ahn, H.-S.; Zubarev, E. R.; Tsukruk, V. V. Microtribological and Nanomechanical Properties of Switchable Y-Shaped Amphiphilic Polymer Brushes. *Adv. Funct. Mater.* **2005**, *15*, 1529–1540.
58. Kozlovskaya, V.; Kharlampieva, E.; Mansfield, M. L.; Sukhishvili, S. A. Poly(methacrylic acid) Hydrogel Films and Capsules: Response to pH and Ionic Strength, and Encapsulation of Macromolecules. *Chem. Mater.* **2006**, *18*, 328–336.
59. Kozlovskaya, V.; Ok, S.; Sousa, A.; Libera, M.; Sukhishvili, S. A. Hydrogen-Bonded Polymer Capsules Formed by Layer-by-Layer Self-Assembly. *Macromolecules* **2003**, *36*, 8590–8592.
60. Markutsya, S.; Jiang, C.; Pikus, Y.; Tsukruk, V. V. Freely Suspended Layer-by-Layer Nanomembranes: Testing Micromechanical Properties. *Adv. Funct. Mater.* **2005**, *15*, 771–780.
61. Sukhishvili, S. A.; Kharlampieva, E.; Izumrudov, V. Where Polyelectrolyte Multilayers and Polyelectrolyte Complexes Meet. *Macromolecules* **2006**, *39*, 8873–8881.
62. Shackelford, J. F.; William, A.; Juns, P. *Materials Science and Engineering Handbook*, 2nd ed.; CRC Press: Boca Raton, FL, 1994.
63. Fery, A.; Weinkamer, R. Mechanical Properties of Micro- and Nanocapsules: Single-Capsule Measurements. *Polymer* **2007**, *48*, 7221–7235.
64. Lulevich, V. V.; Andrienko, D.; Vinogradova, O. I. Elasticity of Polyelectrolyte Multilayer Microcapsules. *J. Chem. Phys.* **2004**, *120*, 3822–3826.
65. Peleshanko, S.; Julian, M. D.; Ornatska, M.; McConney, M. E.; LeMieux, M. C.; Chen, N.; Tucker, C.; Yang, Y.; Liu, C.; Humphrey, J. A. C.; Tsukruk, V. V. Hydrogel-Encapsulated Microfabricated Haircells Mimicking Fish Cupula Neuro-mast. *Adv. Mater.* **2007**, *19*, 2903–2909.
66. Elsner, N.; Kozlovskaya, V.; Sukhishvili, S. A.; Fery, A. pH-Triggered Softening of Crosslinked Hydrogen-Bonded Capsules. *Soft Matter* **2006**, *2*, 966–972.
67. Vinogradova, O. I.; Andrienko, D.; Lulevich, V. V.; Nordschild, S.; Sukhorukov, G. B. Young's Modulus of Polyelectrolyte Multilayers from Microcapsule Swelling. *Macromolecules* **2004**, *37*, 1113–1117.
68. Wilson, J.; Cui, W.; Chaikof, E. L. Layer-by-Layer Assembly of a Conformal Nanothin PEG Coating for Intraportal Islet Transplantation. *Nano Lett.* **2008**, *8*, 1940–1948.
69. Chanana, M.; Gliozi, A.; Diaspro, A.; Chodnevskaja, I.; Huewel, S.; Moskalenko, V.; Ulrichs, K.; Galla, H. J.; Krol, S. Interaction of Polyelectrolytes and Their Composites with Living Cells. *Nano Lett.* **2005**, *5*, 2605–2612.
70. Franz, B.; Balkundi, S.; Dahl, C.; Lvov, Y. M.; Prange, A. Layer-by-Layer Nano-Encapsulation of Microbes: Controlled Cell Surface Modification and Investigation of Substrate Uptake in Bacteria. *Macromol. Biosci.* **2010**, *10*, 164–172.
71. Koguma, I.; Sugita, K.; Saito, K.; Sugo, T. Multilayer Binding of Proteins to Polymer Chains Grafted onto Porous Hollow-Fiber Membranes Containing Different Anion-Exchange Groups. *Biotechnol. Prog.* **2000**, *16*, 456–461.
72. Dash, Ph. R.; Read, M. L.; Fisher, K. D.; Howard, K. A.; Wolfert, M.; Oupicky, D.; Subr, V.; Strohalm, J.; Ulbrich, K.; Seymour, L. W. Decreased Binding to Proteins and Cells of Polymeric Gene Delivery Vectors Surface Modified with a Multivalent Hydrophilic Polymer and Retargeting through Attachment of Transferrin. *J. Biol. Chem.* **2000**, *275*, 3793–3802.
73. Steffens, G. C. M.; Nothdurft, L.; Buse, G.; Thissen, H.; Hocker, H.; Klee, D. High Density Binding of Proteins and Peptides to Poly( $\text{D,L}$ -lactide) Grafted with Polyacrylic Acid. *Biomaterials* **2002**, *23*, 3523–3531.
74. <http://www.biovision.com/manuals/K501.pdf>, <http://www.biovision.com/manuals/K303.pdf>.
75. Kozlovskaya, V.; Shamaev, A.; Sukhishvili, S. A. Tuning Swelling pH and Permeability of Hydrogel Multilayer Capsules. *Soft Matter* **2008**, *4*, 1499–1507.
76. Kharlampieva, E.; Kozlovskaya, V.; Wallet, B.; Shevchenko, V. V.; Naik, R. R.; Vaia, R.; Kaplan, D. L.; Tsukruk, V. V. Co-cross-linking Silk Matrices with Silica Nanostructures for Robust Ultrathin Nanocomposites. *ACS Nano* **2010**, *4*, 7053–7063.